THE JOURNAL OF PHYSICAL CHEMISTRY B
A JOURNAL OF THE AMERICAN CHEMICAL SOCIETY

pubs.acs.org/JPCB
Article

Anion-Dependent Strength Scale of Interactions in Ionic Liquids from X-ray Photoelectron Spectroscopy, Ab Initio Molecular Dynamics, and Density Functional Theory

Published as part of The Journal of Physical Chemistry B virtual special issue "COIL-9:9th Congress on Ionic Liquids".

Ekaterina Gousseva, Frances K. Towers Tompkins, Jake M. Seymour, Lewis G. Parker, Coby J. Clarke, Robert G. Palgrave, Roger A. Bennett, Ricardo Grau-Crespo, and Kevin R. J. Lovelock*

Cite This: J. Phys. Chem. B 2024, 128, 5030−5043

ABSTRACT: Using a combination of experiments and calculations, we have gained new insights into the nature of anion−cation interactions in ionic liquids (ILs). An X-ray photoelectron spectroscopy (XPS)-derived anion-dependent electrostatic interaction strength scale, determined using XPS core-level binding energies for IL cations, is presented here for 39 different anions, with at least 18 new anions included. Linear correlations of experimental XPS core-level binding energies for IL cations with (a) calculated core binding energies (ab initio molecular dynamics (AIMD) simulations were used to generate high-quality model IL structures followed by single-point density functional theory (DFT) to obtain calculated core binding energies), (b) experimental XPS core-level binding energies for IL anions, and (c) other anion-dependent interaction strength scales led to three main conclusions. First, the effect of different anions on the cation can be related to ground-state interactions. Second, the variations of anion-dependent interactions with the identity of the anion are best rationalized in terms of electrostatic interactions and not occupied valence state/unoccupied valence state interactions or polarizability-driven interactions. Therefore, the XPS-derived anion-dependent interaction strength scale can be explained using a simple electrostatic model based on electrostatic site potentials. Third, anion−probe interactions, irrespective of the identity of the probe, are primarily electrostatic, meaning that our electrostatic interaction strength scale captures some inherent, intrinsic property of anions independent of the probe used to measure the interaction strength scale.

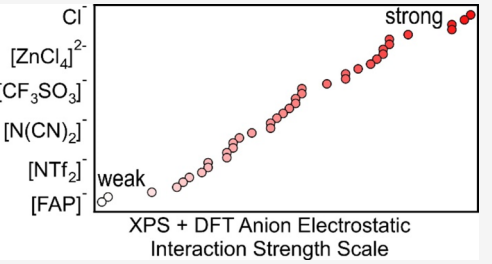

1. INTRODUCTION

In ionic liquids (ILs), liquids composed solely of ions, anion−cation interactions are very important,[1,2] as they heavily influence both macroscopic and mesoscopic properties including static (e.g., density, vapor pressure, surface tension, solubility) and transport properties (e.g., conductivity, viscosity, and chemical reactivity). The drivers for these properties need to be understood to push forward the many potential applications of ILs: electrochemical energy storage,[3−5] metal electrodeposition,[6] sensors,[7] gas capture and storage,[8] solvents for catalysis,[9] and metal extraction and recycling.[10,11] Therefore, understanding anion−cation interactions is vital. However, identifying and classifying anion−cation interactions is very challenging; experimental evidence is relatively scarce, and the size and complexity of IL anions and cations make quantum chemical studies of anion−cation interactions difficult.

Experimental X-ray photoelectron spectroscopy (XPS)[12−14] of ILs with the cation 1-octyl-3-methylimidazolium ($[C_8C_1Im]^+$, Figure 1a) and ∼25 different anions $[A]^-$ has shown anion-dependent differences for experimental cation core binding energies, E_B(cation core,exp.),[15−18] giving an XPS-derived anion-dependent interaction scale. The same anion-dependent interaction scale has been demonstrated for a range of further organic cations, including both aromatic[15,19,20] and nonaromatic (e.g., tetradecyl(trihexyl)phosphonium, $[P_{6,6,6,14}]^+$, Figure 1b).[21,22] However, the nature of this anion-dependent interaction is not yet understood.

The anion-dependent E_B(cation core,exp.) differences can be due to a ground-state effect (called the initial-state effect in the XPS community), which is related to the bonding/interactions, or due to the core-hole created by the photoemission process in XPS (called the final-state effect in the XPS community), which is related to relaxation of other

Received: January 17, 2024
Revised: April 22, 2024
Accepted: April 22, 2024
Published: May 10, 2024

https://doi.org/10.1021/acs.jpcb.4c00362
J. Phys. Chem. B 2024, 128, 5030−5043

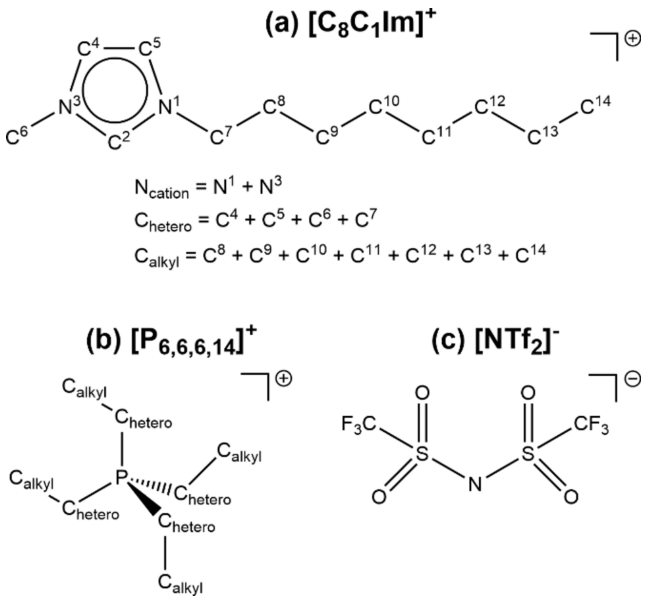

Figure 1. Structure of key ions with labels relevant to XPS: (a) 1-octyl-3-methylimidazolium = $[C_8C_1Im]^+$, (b) tetradecyl(trihexyl)-phosphonium = $[P_{6,6,6,14}]^+$, and (c) bis[(trifluoromethane)sulfonyl]-imide = $[NTf_2]^-$.

core and valence electrons after the core-hole is created but before photoemission.[23,24] In the initial-state interpretation, E_B(cation core,exp.) differences can be understood in terms of the electrostatic site potentials and the charge potential model,[25,26] where greater electron-withdrawing power of substituents/ligands/counterions surrounding an atom corresponds to larger E_B for that atom.[25] In the final-state interpretation, E_B(cation core,exp.) differences can be understood in terms of the ability of electrons surrounding the atom with the core-hole to react to the creation of that core-hole, akin to the polarizability of the neighboring atoms. Almost all experimental XPS studies of ILs have assumed that the initial-state interpretation holds.[15−22,27−64] Calculated core binding energies, E_B(core,calc.), for a small number of IL ion pairs in the initial-state approximation (without a core-hole)[31] and the final-state approximation (with a core-hole)[37,65] gave reasonable matches to experimental data, and comparisons of E_B(core,exp.) and calculated atomic charges gave acceptable correlations.[15,38,43,44] Recently, ab initio molecular dynamics (AIMD) calculations (to obtain structures that are more representative of ILs in the liquid phase) followed by single-point density functional theory (DFT) of $[C_4C_1Im][SCN]$ suggested that initial-state effects dominated local variations of E_B(core) within the IL. This conclusion was based on the fact that initial-state calculations gave excellent visual matches for the N 1s and final-state calculations for S 2p and N 1s in the anion $[SCN]^-$ gave the same trends as initial-state calculations.[66] However, no results were presented on anion-dependent interactions. Hence, whether the XPS-derived anion-dependent interaction strength scale is due to initial-state effects or final-state effects is still an open question.

The molecular origin of this XPS-derived anion-dependent interaction was suggested, based on gas phase ion pair calculations for three ILs ($[C_8C_1Im]^+$ with $[NTf_2]^-$ (bis-[(trifluoromethane)sulfonyl]imide, Figure 1c), $[BF_4]^-$, and Cl^-), to be a ground-state anion-dependent anion-to-cation electron density donation through orbital mixing between the anion and cation, termed charge transfer.[15,67] Experimental XPS results for the nonmethylated versus methylated imidazolium cations (at the C^2 position, Figure 1a) ruled out a hydrogen bonding interaction to explain the XPS-derived anion-dependent interaction scale.[15] However, an explanation based on larger-scale calculations of the molecular origin of the XPS-derived anion-dependent interaction scale is yet to be made.

Excellent linear correlations have been found between the XPS-derived anion-dependent interaction scale and a ultraviolet−visible (UV−vis) spectroscopy-derived anion-dependent hydrogen-bond acceptor interaction scale (Kamlet−Taft β values).[15,16] A nonlinear relationship was reported for the XPS-derived anion-dependent interaction scale and an electron donor ability scale (^{23}Na NMR spectroscopy of Na^+ dissolved in different ILs).[68] There are far more ILs available now, so attempts at finding linear correlations can be more robust. There are a number of interaction scales available in the literature for the strength of anion−cation interactions, e.g., ^{1}H NMR spectroscopy of C^2−H of $[C_4C_1Im]^+$ in a molecular solvent,[69,70] an electron donor scale from UV−vis spectroscopy of a Cu^{II} cationic complex dissolved in different ILs,[70] and ion pair calculations of hydrogen-bond strength,[71] and also for the strength of anion−neutral molecule interactions (more often called Lewis basicity/hydrogen-bond acceptor ability/electron donor number).[69,72−78] It is currently unclear whether these scales capture the same interactions as the XPS-derived interaction scale.

In this study, we intend to primarily answer four questions. (i) Where do key anions, e.g., $[SCN]^-$ and $[HSO_4]^-$, come on the XPS-derived interaction strength scale? (ii) Is the XPS-derived anion-dependent interaction strength scale due to initial-state (i.e., ground-state) effects or final-state effects? (iii) What is the best explanation for the XPS-derived anion-dependent interaction scale, e.g., occupied valence state/unoccupied valence state interaction, polarizability, or electrostatic interactions? (iv) Does the experimental XPS-derived interaction strength scale correlate with other measures of the strength of anion−cation interactions or the strength of anion−neutral molecule interactions? We answered these questions using a combination of core XPS, valence XPS, and AIMD plus DFT to obtain realistic structures of ILs, followed by single-point DFT calculations to obtain E_B(core,calc.).

2. METHODS

2.1. Ionic Liquid Synthesis. Details of IL synthesis/purchase for the six ILs included here where core XPS was previously unpublished ($[C_8C_1Im]_2[Bi_2Cl_8]$, $[C_8C_1Im][CF_3CO_2]$, $[C_8C_1Im][SnBr_3]$, $[C_8C_1Im]_2[Zn_3Cl_8]$, $[C_8C_1Im][FSI]$ where $[FSI]^-$ = bis(fluorosulfonyl)imide, $[C_8C_1Im][InBr_4]$) are given in Section 1 in the ESI. The synthetic procedure for $[C_8C_1Im]_2[Zn_3Cl_8]$ was also given in ref 79.

2.2. X-ray Photoelectron Spectroscopy. Laboratory-based XPS was recorded for six ILs ($[C_8C_1Im]_2[Bi_2Cl_8]$, $[C_8C_1Im][CF_3CO_2]$, $[C_8C_1Im][SnBr_3]$, $[C_8C_1Im]_2[Zn_3Cl_8]$, $[C_8C_1Im][FSI]$, $[C_8C_1Im][InBr_4]$) at the University of Reading on a Thermo Scientific ESCALAB 250 monochromated Al Kα source ($h\nu$ = 1486.6 eV) spectrometer. A drop of IL was placed directly onto a stainless steel sample plate. This sample was placed in a loadlock, and the pressure was reduced to 10^{-7} mbar by pumping down for >6 h. After attaining the required pressure, the IL was transferred to the analysis

https://doi.org/10.1021/acs.jpcb.4c00362
J. Phys. Chem. B 2024, 128, 5030−5043

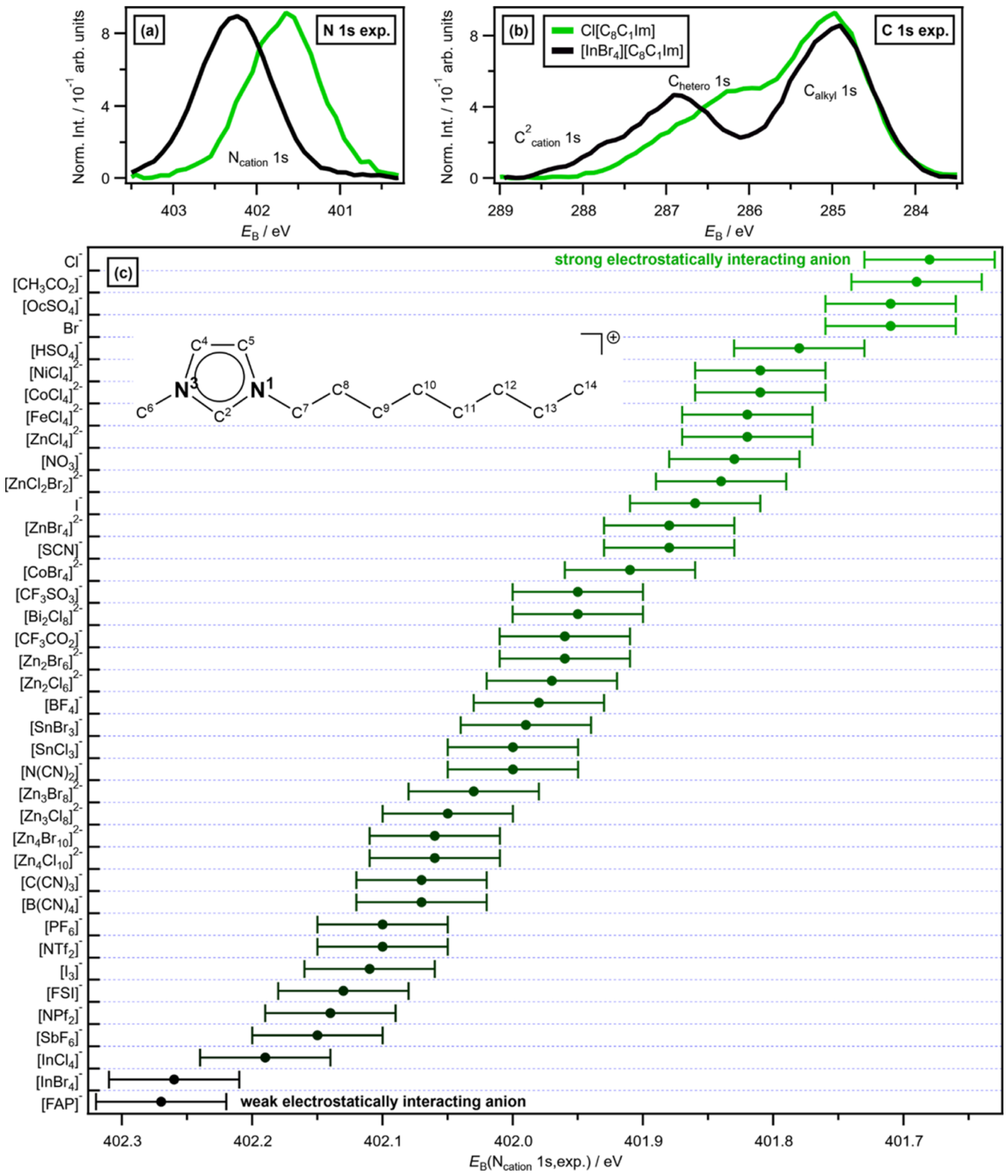

Figure 2. Experimental XPS for $[C_8C_1Im][A]$ where $[A]^-$ = Cl^- and $[InBr_4]^-$: (a) experimental N 1s XPS; (b) experimental C 1s XPS. (c) $E_B(N_{cation}$ 1s,exp.) for 39 different anions measured for $[C_nC_1Im][A]$ (see Table S5 in the ESI for the numerical values). The estimated uncertainty is ±0.05 eV. Data from this paper apart from $[NO_3]^-$,[15] $[NPf_2]^-$,[15] $[CH_3CO_2]^-$,[33] $[SbF_6]^-$,[36] and $[I_3]^-$.[18] Large $E_B(N_{cation}$ 1s,exp.) = weak electrostatically interacting anion (black) and small $E_B(N_{cation}$ 1s,exp.) = strong electrostatically interacting anion (green). Inset in (c): structure of the cation 1-octyl-3-methylimidazolium, $[C_8C_1Im]^+$, with two N_{cation} atoms highlighted.

chamber. Etching was carried out using a rastered 500 eV Ar^+ ion beam (20 s for $[C_8C_1Im]_2[Bi_2Cl_8]$ and 500 s for $[C_8C_1Im]_2[Zn_3Cl_8]$). For both $[C_8C_1Im][CF_3CO_2]$ and $[C_8C_1Im]_2[Zn_3Cl_8]$, an area scan was performed to minimize sample charging/damage. Acquisition parameters were matched to give comparable energy resolution with data

https://doi.org/10.1021/acs.jpcb.4c00362
J. Phys. Chem. B 2024, 128, 5030−5043

already published; a pass energy of 20 eV was used for core-levels.

All experimental XP spectra were fitted using CasaXPS software. Fitting was carried out using a Shirley background and GL30 line shapes (70% Gaussian, 30% Lorentzian). Peak constraints used are outlined in Section 2 in the ESI. Relative sensitivity factors from ref 80 were used to ensure the experimental stoichiometries matched the nominal stoichiometries.

All XPS E_B(core,exp.) values were shifted relative to $E_B(C_{alkyl}$ 1s,exp.) = constant value, chosen as $E_B(C_{alkyl}$ 1s,exp.) = 285.00 eV here, as standard for ILs;[15,30,81] more details on charge referencing experimental XPS of ILs are given in Section 2 in the ESI. From multiple measurements of the same IL, we have found that the uncertainty in $E_B(N_{cation}$ 1s,exp.) is smaller than given in references published in 2010 and 2011;[15,30] here, we have used ±0.05 eV for uncertainty in $E_B(N_{cation}$ 1s,exp.).

$E_B(N_{cation}$ 1s,exp.) for $[C_8C_1Im]^+$-based ILs are used as the primary measure of the anion-dependent interaction strength (e.g., Figure 2a,c). $E_B(C_{hetero}$ 1s,exp.) and $E_B(C^2$ 1s,exp.) can also be used as a secondary measure of the anion-dependent interaction strength (Figure 2b), although $E_B(N_{cation}$ 1s,exp.) is usually used, as C_{anion} 1s peaks can overlap with C_{hetero} 1s and C^2 1s peaks, e.g., for $[SCN]^-$-based ILs,[66] making fitting more challenging when obtaining $E_B(C_{hetero}$ 1s,exp.) and $E_B(C^2$ 1s,exp.) than $E_B(N_{cation}$ 1s,exp.).

A major difference between the measurement conditions for the XPS-derived interaction scale and the other eight interaction scales discussed above is that the IL XPS measurements are made under ultrahigh vacuum (UHV) conditions. These UHV conditions mean that residual molecular solvents will have vaporized prior to XPS measurements, giving ultrapure samples from a molecular solvent contamination perspective. Furthermore, the element-specific nature of XPS means that a number of ionic impurities, e.g., Na^+, can be observed. Therefore, we can have very high confidence in the purity of our ILs for the XPS measurements.

2.3. Ab Initio Molecular Dynamics. The ILs $[C_8C_1Im][SCN]$, $[C_8C_1Im][NTf_2]$, and $[C_8C_1Im]Cl$ were each simulated using a 32-ion pair model with densities and temperatures, as listed in Table 1. The AIMD was calculated with the Quickstep code in CP2K, from the Gaussian and plane wave method (GPW) and using the direct inversion in iterative subspace (DIIS) technique. Pre-equilibration was performed using the classical force field DREIDING, and then the AIMD simulation was run at a time step of 1 fs for 30 ps. All simulations were controlled by a Nosé thermostat in the canonical NVT ensemble. The Perdew–Burke–Ernzerhof (PBE) functional[82] was applied, with Grimme's D2 corrections[83,84] to account for dispersion interactions. An increased simulation temperature was used (Table 1) to reduce the viscosity in the system and allow for equilibrium to be achieved faster, thus reducing the computational cost of the calculation while preventing thermal decomposition.

Table 1. Temperature and Density Used for Each Ionic Liquid

ionic liquid	temperature/K	density/g cm^{-3}
$[C_8C_1Im][SCN]$	398	0.89
$[C_8C_1Im][NTf_2]$	398	1.32
$[C_8C_1Im]Cl$	498	1.01

2.4. Core-Level Binding Energy and Electrostatic Site Potential Calculations. Calculations of the E_B(core,calc.) were performed using the Vienna Ab initio Simulation Package (VASP).[85] Three configurations of the average energies calculated in AIMD for each IL were chosen to calculate the E_B values across the 96-ion pairs (3 × 32-ion pairs). The PBE exchange-correlation functional was employed, and the core–valence electron interactions were described using the projector-augmented wave (PAW) potentials.[86,87] The kinetic energy cutoff in the plane wave basis set expansion was set to 400 eV for all ILs. All core-level energies were calculated using the initial-state approximation.

To produce the calculated XP spectra (Figures 3 and 4), a Gaussian–Lorentzian Product (GLP) function was applied to each calculated E_B data point for each core-level using eq 1 and then summed to produce calculated XPS data. The mixing parameter, m, was set to 0.3, as in line with experimental peak fitting, and the function width, F, was set to 0.7 eV.

$$\mathrm{GLP}(x;\,F,\,E,\,m) = \frac{\exp\left[-4\ln 2(1-m)\frac{(x-E)^2}{F^2}\right]}{\left[1+4m\frac{(x-E)^2}{F^2}\right]} \quad (1)$$

To produce the calculated E_B used in Figure 5, an average was taken of the relevant atoms for all three configurations of each IL, i.e., 3 × 32 × n E_B values, where n reflects the different number of atoms for each grouping (e.g., n = 2 for N_{cation} for each IL ion pair).

Electrostatic site potentials were taken from VASP version 6.4.1, where the average of the electrostatic potential is taken from the core of an atom at a given position. To produce the average calculated electrostatic site potentials used in Figure 5d–f, e.g., the N_{cation} electrostatic site potential for each IL, the same averaging method was used as for E_B.

2.5. Aligning Calculated XPS and Electrostatic Site Potential Data. Both E_B(core,calc.) and calculated electrostatic site potentials need to be aligned to allow comparison, as the nature of the AIMD plus DFT bulk IL calculation method used here does not give a simple reference, e.g., there is no vacuum level.

To allow comparisons of our calculated XPS data to our experimental core XPS data, calculated XPS data were aligned with our chosen internal energy reference, $E_B(C_{alkyl}$ 1s,calc.) = 285.00 eV. The average $E_B(C_{alkyl}$ 1s,calc.) value for each IL was shifted to match 285.00 eV for calculated XP spectra, the average E_B(core,calc.) values, and the 3 × 32 × n E_B(core,calc.) values; E_B(core,calc.) for other core-levels (e.g., N 1s) were shifted the same for that particular IL. Hence, only relative E_B values are meaningful; absolute values are not considered here, only the difference between binding energies, ΔE_B. Therefore, $E_B(C_{alkyl}$ 1s,exp.) and $E_B(C_{alkyl}$ 1s,calc.) (Figures 2b, 3b,d,f, and 4a) match perfectly, as they are charge referenced to match at $E_B(C_{alkyl}$ 1s) = 285.00 eV.

The average calculated electrostatic site potentials were set to a common reference, chosen as C_{alkyl} electrostatic site potential = 54.26 V for the average C_{alkyl} site potential of C^8 to C^{14} for $[C_8C_1Im][SCN]$ (Figure 1a for the structure).

3. RESULTS AND DISCUSSION

3.1. XPS-Derived Anion-Dependent Interaction Strength Scale for 39 Different Anions. An XPS-derived anion-dependent interaction strength scale for 39 different anions is presented here (Figure 2c),[15,16,18,33] with at least 18

https://doi.org/10.1021/acs.jpcb.4c00362
J. Phys. Chem. B 2024, 128, 5030–5043

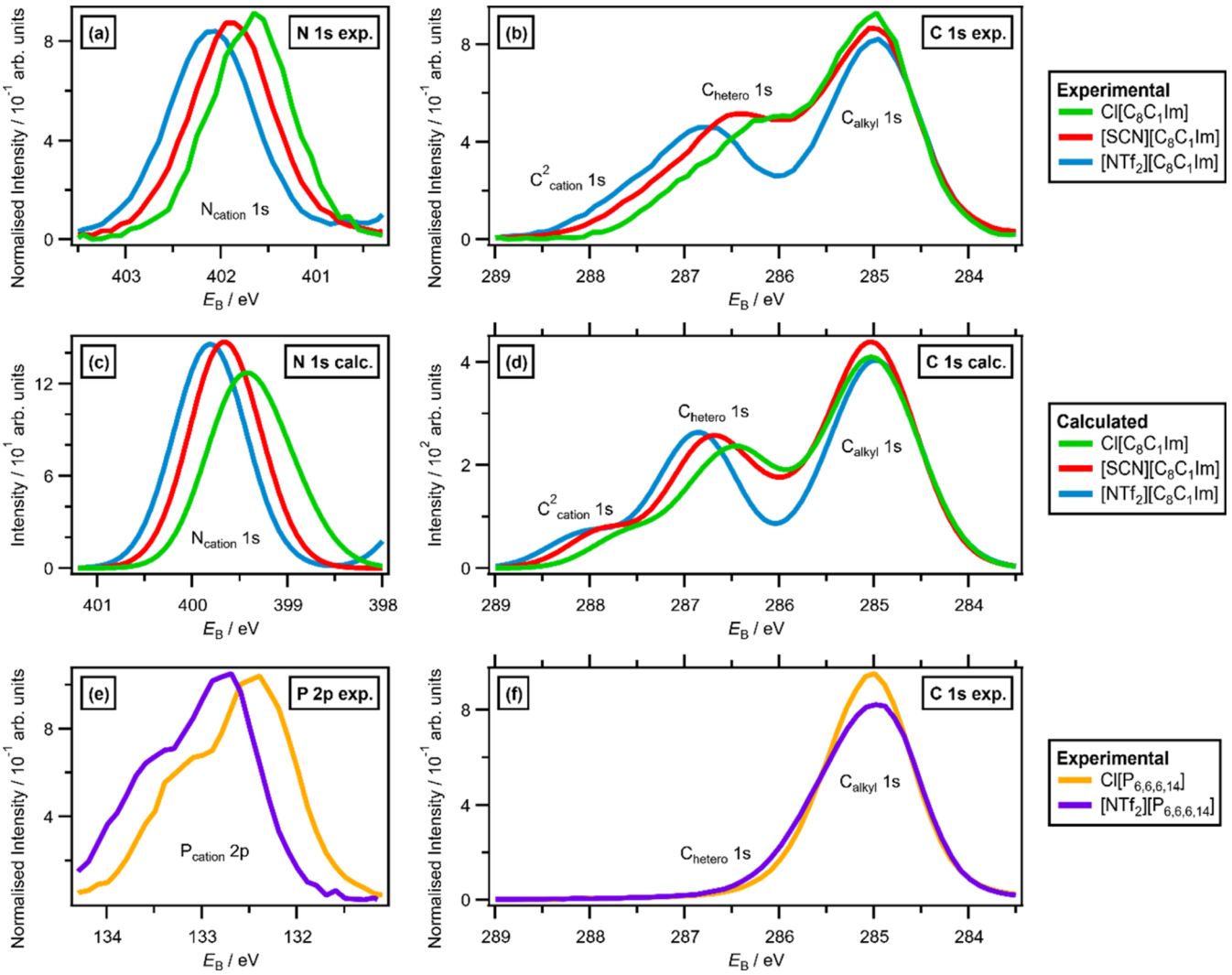

Figure 3. Experimental and calculated XPS for $[C_8C_1Im][A]$, where $[A]^-$ = Cl^-, $[SCN]^-$, and $[NTf_2]^-$: (a) experimental N 1s XPS, (b) experimental C 1s XPS, (c) calculated N 1s XPS for three configurations of each IL (fwhm = 0.7 eV), and (d) calculated C 1s XPS for three configurations of each IL (fwhm = 0.7 eV). Experimental XPS for $[P_{6,6,6,14}][A]$,where $[A]^-$ = Cl^- and $[NTf_2]^-$: (e) experimental P 2p XPS and (f) experimental C 1s XPS.

anions placed on the scale for the first time, e.g., the weakly interacting $[FSI]^-$ anion, which is very important for batteries.[88] A major advantage of this XPS-derived scale is the ability to measure both ILs that are inherently colored (a problem for UV−vis spectroscopy measurements, e.g., $[Bi_2Cl_8]^{2-}$) and ILs that are magnetic (a problem for NMR spectroscopy, e.g., $[CoBr_4]^{2-}$). Two examples of placing anions on the XPS-derived interaction strength scale are given in Figure 2a,b: Cl^- and $[InBr_4]^-$. Cl^- has been measured previously using XPS and placed on the interaction scale as among the most strongly interacting anions for ILs (Figure 2c).[15] XPS data are published here that allow the placement of the key cyano-based anions on the XPS-derived interaction scale for the first time. Other new anions include $[HSO_4]^-$ and halometallate anions, which span a wide range of anion interaction strengths from strong, e.g., $[MCl_4]^{2-}$ (where M = Co^{2+}, Ni^{2+}, Fe^{2+}, Zn^{2+}), to weak, e.g., $[InCl_4]^-$ and $[InBr_4]^-$ (Figure 2c); $[FAP]^-$ (tris(pentafluoroethyl)-trifluorophosphate) is the most weakly interacting anion measured using XPS but is the same as $[InBr_4]^-$ within the uncertainty (Figure 2c). Perhaps somewhat surprisingly, the magnitude of the anion charge is not a major determinant in the anion interaction strength; doubly charged anions are not always strongly interacting (e.g., $[Zn_4Cl_{10}]^{2-}$; Figure 2c[89]), while singly charged anions are not always weakly interacting (e.g., Cl^- and $[CH_3CO_2]^-$ (acetate); Figure 2c).

The maximum $\Delta E_B(N_{cation}$ 1s,exp.) for $[C_8C_1Im][A]$ with different $[A]^-$ was 0.59 eV (402.27 eV for $[FAP]^-$ to 401.68 eV for Cl^-; Figure 2c). This $\Delta E_B(N_{cation}$ 1s,exp.) value is very small compared to the largest ΔE_B(N 1s,exp.) in our XPS data set for all ILs, $\Delta E_B(N_{anion}$ 1s,exp.) = 8.66 eV for $[NO_3]^-$ versus $[SCN]^-$ (caused by the difference in covalent bonding in these anions; Figure S13 in the ESI). Moreover, $\Delta E_B(N_{cation}$ 1s,exp.) was 0.80 eV for $[C_8C_1Im]^+$ versus $[N_{4,1,1,1}]^+$. These and other comparisons (Figure S13 in the ESI) highlight that the change in $\Delta E_B(N_{cation}$ 1s,exp.) for $[C_8C_1Im][A]$ with different $[A]^-$ is smaller than changes caused by differences in covalent bonding in individual ions.

3.2. XPS-Derived Anion-Dependent Interactions: Ground-State Explanation. Our AIMD plus (ground-state) DFT calculations can be validated against our experimental XPS data. First, intramolecular evidence: for

https://doi.org/10.1021/acs.jpcb.4c00362
J. Phys. Chem. B 2024, 128, 5030−5043

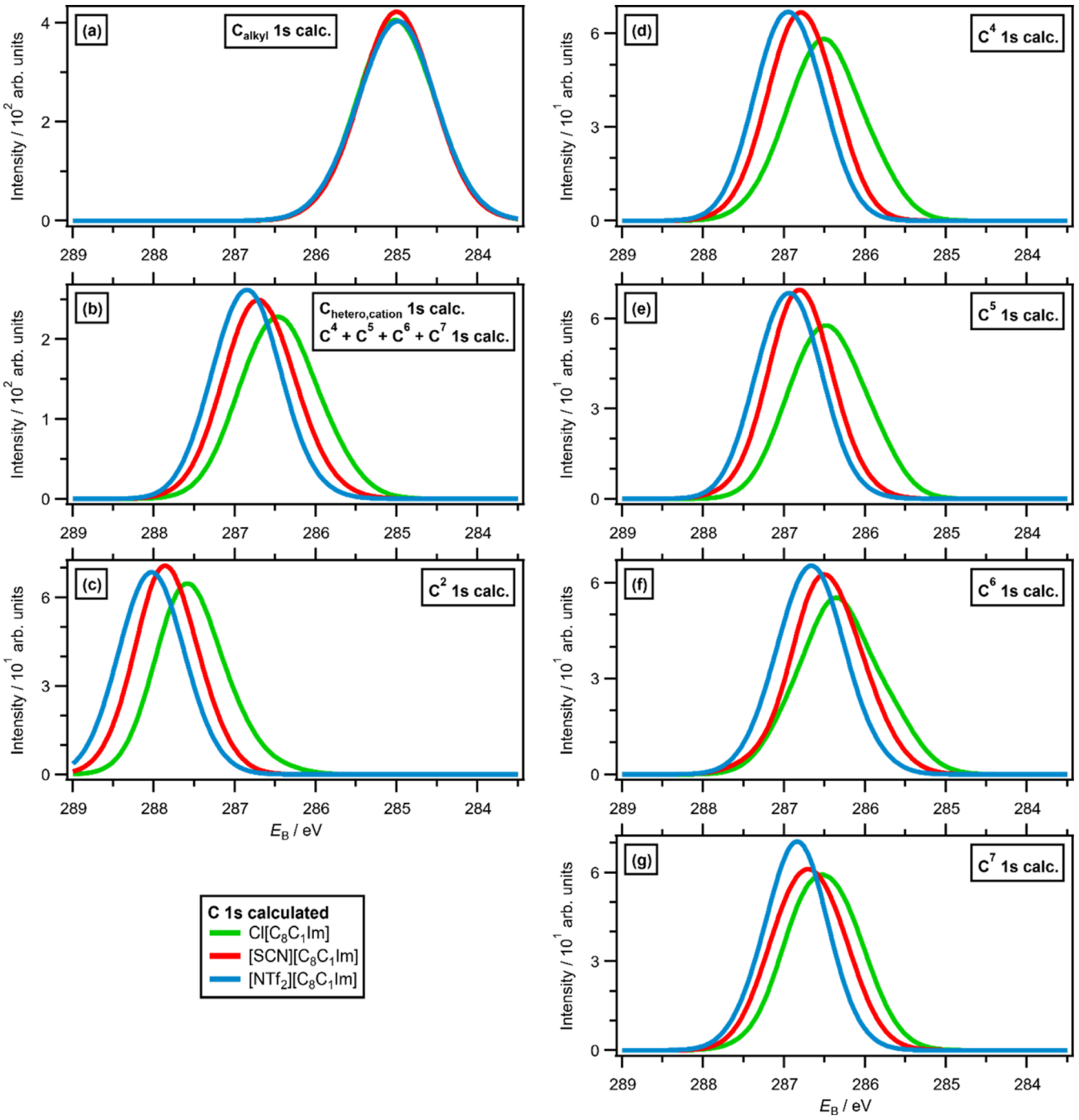

Figure 4. Calculated C 1s XPS for $[C_8C_1Im][A]$, where $[A]^- = Cl^-$, $[SCN]^-$, and $[NTf_2]^-$ for three configurations of each IL (fwhm = 0.7 eV): (a) C_{alkyl} 1s XPS, (b) C_{hetero} 1s XPS, (c) C^2 1s XPS, (d) C^4 1s XPS, (e) C^5 1s XPS, (f) C^6 1s XPS, and (g) C^7 1s XPS.

XPS of all $[C_nC_1Im]^+$-based ILs, the E_B order of $E_B(C^2\ 1s) > E_B(C_{hetero}\ 1s) > E_B(C_{alkyl}\ 1s)$ from both experimental and calculated XPS (Figures 2b and 3b,d) matches to the electronegativity of the atom covalently bonded to the carbon atom in question, i.e., C^2 has two C−N bonds, all C_{hetero} have one C−N bond, and C_{alkyl} has no C−N bonds (only C−C and C−H). This observation is exactly as expected based on the XPS literature.[25,26,90,91] Second, interion evidence: anion−cation interion interactions between the $[C_8C_1Im]^+$ cation and the anions are captured. For $[C_8C_1Im][NTf_2]$ (both N 1s and C 1s) and $[C_8C_1Im][SCN]$ (N 1s) (both N 1s and C 1s for $[C_4C_1Im][SCN]$ in ref 66), E_B(anion core,exp.) minus E_B(cation core,exp.) matches very well to E_B(anion core,calc.) minus E_B(cation core,calc.) (Figure S14 in the ESI).

There are excellent matches between the experimental and calculated XPS for cation-based contributions (Figures 3a−d and 5a−5c) for $[C_8C_1Im][A]$ (where $[A]^- = [NTf_2]^-$, $[SCN]^-$, Cl^-). For N_{cation} 1s XPS, there is an excellent match of the experimental and calculated N_{cation} 1s XPS (Figure 3a,c respectively) for $[C_8C_1Im][A]$ (where $[A]^- = [NTf_2]^-$, $[SCN]^-$, Cl^-). Both experiments and calculations find the same order for $E_B(N_{cation}\ 1s,exp.)$ of $[NTf_2]^- > [SCN]^- > Cl^-$ (see Figure 2c for comparisons to values for other anions). A comparison of the experimental versus

https://doi.org/10.1021/acs.jpcb.4c00362
J. Phys. Chem. B 2024, 128, 5030−5043

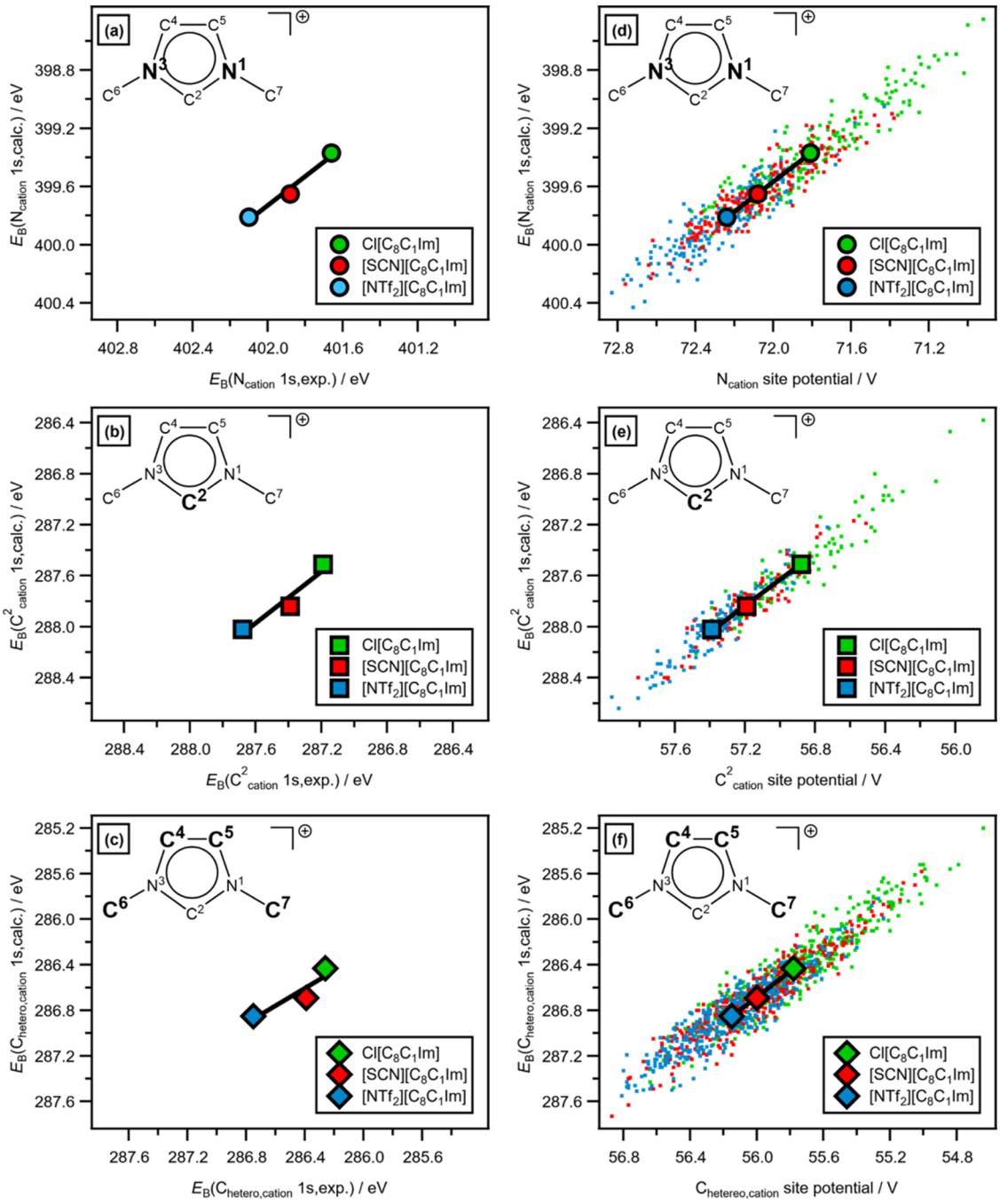

Figure 5. Experimental and calculated XPS E_B and site potential data for $[C_8C_1Im][A]$, where $[A]^-$ = Cl^-, $[SCN]^-$, and $[NTf_2]^-$: (a) average $E_B(N_{cation}$ 1s,calc.) (for three configurations of each IL) versus $E_B(N_{cation}$ 1s,exp.), (b) average $E_B(C^2_{cation}$ 1s,calc.) (for three configurations of each IL) versus $E_B(C^2_{cation}$ 1s,exp.), and (c) average $E_B(C_{hetero}$ 1s,calc.) (for three configurations of each IL) versus $E_B(C_{hetero}$ 1s,exp.). Calculated XPS E_B and site potential data (both all individual atoms and the average for three configurations of each IL): (d) $E_B(N_{cation}$ 1s,calc.) versus N_{cation} site potential, (e) $E_B(C^2$ 1s,calc.) versus C^2 site potential, and (f) $E_B(C_{hetero}$ 1s,calc.) versus C_{hetero} site potential.

calculated C^2_{cation} 1s XPS (Figure 3b,d, respectively) and experimental versus calculated C_{hetero} 1s XPS (Figure 3b,d, respectively) for $[C_8C_1Im][A]$ (where $[A]^-$ = $[NTf_2]^-$, $[SCN]^-$, Cl^-) show the same order of $[NTf_2]^-$ > $[SCN]^-$ > Cl^-, matching the observed order for $E_B(N_{cation}$ 1s,exp.). Breakdowns of C_{hetero} 1s and C^2 1s for $[NTf_2]^-$ versus $[SCN]^-$ versus Cl^- also highlight these trends (Figure 4b,c, respectively). Analysis is slightly more complicated for the $[SCN]^-$ anion for C 1s than N_{cation} 1s because the carbon from the $[SCN]^-$ anion (C_{anion} 1s) contributes in a similar E_B region to C_{hetero} 1s and C_{alkyl} 1s (see experimental evidence for this finding in ref 66); this C_{anion} 1s contribution can be easily separated in the calculated XPS but is more challenging to account for when fitting the experimental XPS.

The magnitude of the E_B shifts in $E_B(N_{cation}$ 1s), $E_B(C^2_{cation}$ 1s), and $E_B(C_{hetero}$ 1s) for $[C_8C_1Im][A]$ (where $[NTf_2]^-$, $[SCN]^-$, and Cl^-) matches well for experimental versus calculated XPS both for the XP spectra (Figure 3a,c, respectively) and for E_B(core) values, with excellent linear correlations of three data points for the average $E_B(N_{cation}$

https://doi.org/10.1021/acs.jpcb.4c00362
J. Phys. Chem. B 2024, 128, 5030−5043

1s,calc.) versus $E_B(N_{cation}$ 1s,exp.) (Figure 5a), and the same plots for $E_B(C^2_{cation}$ 1s) and $E_B(C_{hetero}$ 1s) (Figure 5b,c, respectively).

These observations show that the XPS-derived anion-dependent interaction strength scale for ILs is a ground-state effect (in XPS language, an initial-state effect) and not a product of electron density redistribution after the core-hole is created in XPS (i.e., not an XPS final-state effect). This finding strongly backs the assumption used regularly in the IL XPS literature that initial-state effects dominate E_B shifts for ILs.[15−22,27−29,31−64] Therefore, the effect of different anions on the cation can be related to ground-state differences.

3.3. XPS-Derived Anion-Dependent Interactions: An Electrostatic Explanation for the Cation Changes. The average E_B(core,calc.) linearly correlates with the average calculated electrostatic site potentials, i.e., $E_B(N_{cation}$ 1s,calc.) versus N_{cation} electrostatic site potential (Figure 5b), $E_B(C^2_{cation}$ 1s,calc.) versus C^2_{cation} electrostatic site potential (Figure 5d), and $E_B(C_{hetero,cation}$ 1s,calc.) versus C_{hetero} electrostatic site potential (Figure 5f). Furthermore, E_B(core,exp.) linearly correlates with the average calculated electrostatic site potentials for C^2_{cation}, N_{cation}, and C_{hetero} (Figure S16 in the ESI). For each IL, when all calculated data points are considered rather than the average calculated values, excellent linear correlations are found (for N_{cation}, C^2_{cation}, and C_{hetero} in Figure 5d,e,f, respectively), e.g., for $[C_8C_1Im][SCN]$, when all 192 relevant atoms from three configurations are considered, calculated $E_B(N_{cation}$ 1s,calc.) shows an excellent linear correlation with the N_{cation} electrostatic site potential (Figure 5d). Therefore, it can be concluded that the electrostatic site potentials for all three of the imidazolium ring carbon atoms (C^2, C^4, and C^5), the two imidazolium ring nitrogen atoms (N^1 and N^3) and the two N−CH_2R carbon atoms (C^6 and C^7) are affected by the anion identity in the order $[NTf_2]^-$ > $[SCN]^-$ > Cl^-. This observation that all of these imidazolium-based atoms are affected the same by the different anions is evidence of the dominant role of electrostatic interactions and relative unimportance of occupied valence state/unoccupied valence state interactions, as for interactions involving specific valence states one would expect some atoms, especially the ring atoms, to be affected more than other atoms.

There is an excellent linear correlation between the anion core-level E_B(Cl $2p_{3/2}$,exp.) and $E_B(N_{cation}$ 1s,exp.) for eight Cl-containing ILs (Figure 6a). Furthermore, there is also an excellent linear correlation between the anion core-level E_B(Br $3d_{5/2}$,exp.) and $E_B(N_{cation}$ 1s,exp.) for eight Br-containing ILs (Figure 6b). The R^2 values for both of these linear correlations would be increased by removing the free halide data points (i.e., Cl^- and Br^- anions), potentially due to a different interaction mechanism with the cations for the free halides compared to the halometallate anions. The experimental anion core-level E_B(anion core) can be taken as a measure of the electrostatic site potential at these anion atoms. Therefore, these linear correlations demonstrate that the anion-dependent interaction strength for the Cl- and Br-containing ILs can be explained by electrostatic interactions between the halide atom(s) and both the imidazolium ring and the two N−CH_2R carbon atoms of the cation. Furthermore, a plot of $E_B(O_{anion}$ 1s,exp.) versus $E_B(N_{cation}$ 1s,exp.) for eight O-containing anions gave a reasonable linear correlation (Figure S18 in the ESI), backing up our arguments made for the Cl- and Br-containing anion data sets.

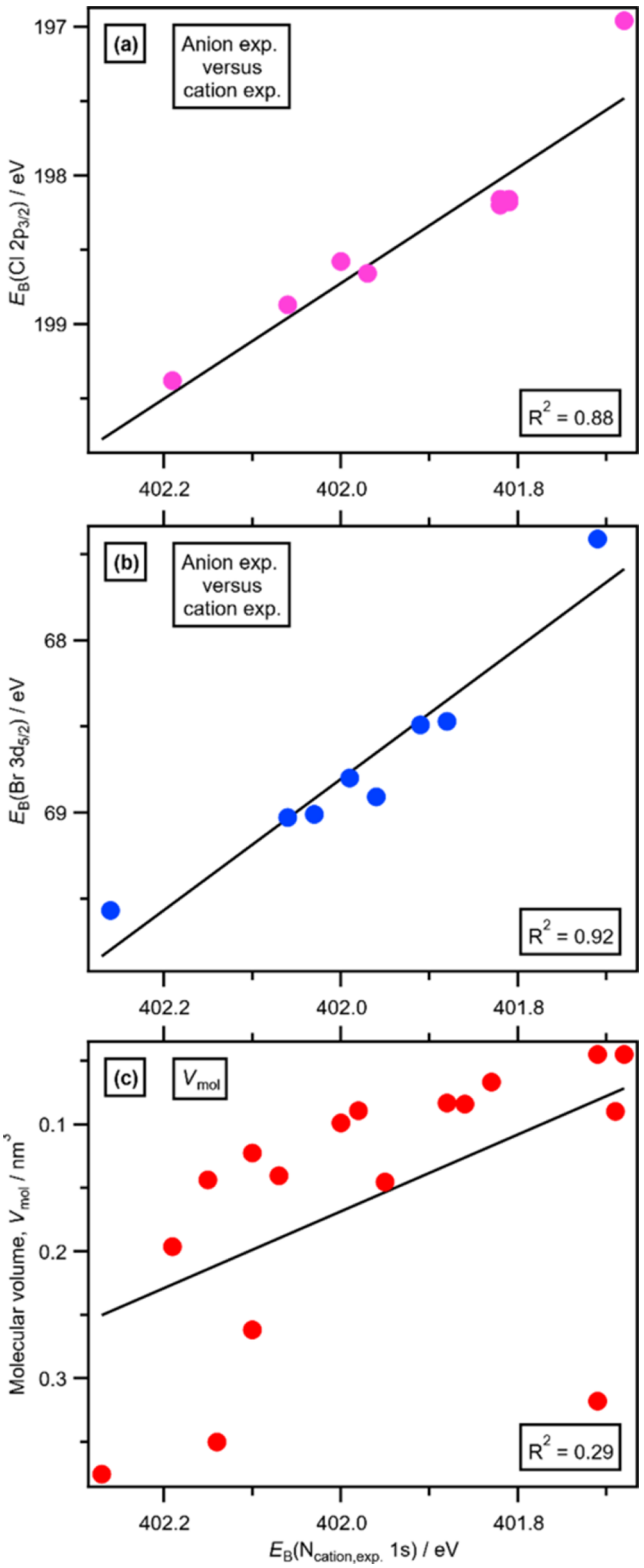

Figure 6. Anion properties plotted against $E_B(N_{cation}$ 1s,exp.): (a) E_B(Cl $2p_{3/2}$,exp.) versus $E_B(N_{cation}$ 1s,exp.) for nine Cl-containing ILs, (b) E_B(Br $3d_{5/2}$,exp.) versus $E_B(N_{cation}$ 1s,exp.) for eight Br-containing ILs, and (c) calculated anion molecular volume, V_{mol}, taken from ref 93 versus $E_B(N_{cation}$ 1s,exp.) for 17 ILs (Table S5 in the ESI for values used).

Beyond the multiple linear correlations between E_B and electrostatic site potential, there are three pieces of evidence to

https://doi.org/10.1021/acs.jpcb.4c00362
J. Phys. Chem. B 2024, 128, 5030−5043

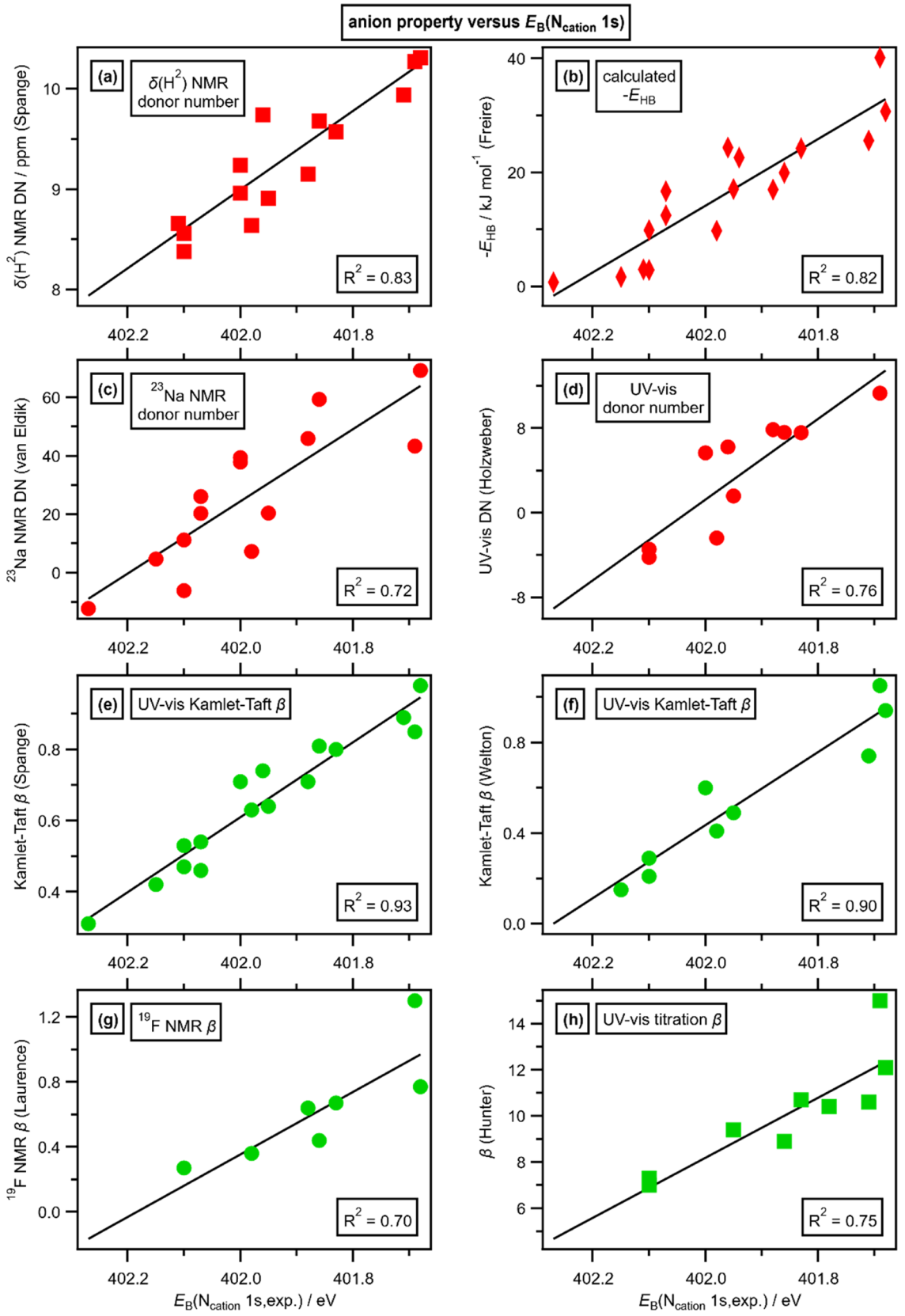

Figure 7. Measures of anion Lewis basicity/electron donor ability/hydrogen-bond acceptor ability plotted against $E_B(N_{cation}\ 1s,exp.)$: (a) electron donor number measured from the chemical shifts $\delta(H)$ of the C^2−H proton by ^{1}H NMR spectroscopy of $[C_4C_1Im][A]$ in the molecular solvent CD_2Cl_2;[69,70] (b) hydrogen-bond basicity calculated using ion pairs in COSMO-RS (COnductor-like Screening MOdel for Real Solvents);[71] (c) anion electron donor numbers measured from the chemical shift $\delta(Na^+)$ by ^{23}Na NMR spectroscopy of $Na[ClO_4]$ dissolved in $[C_4C_1Im][A]$ neat ionic liquids;[68] (d) anion electron donor numbers measured from the peak shift of the copper complex [Cu(acetylacetonate)-(tetramethylethylenediamine)][ClO_4] by UV−vis spectroscopy in $[C_4C_1Im][A]$ neat ionic liquids;[70] (e) Kamlet−Taft hydrogen-bond acceptor

https://doi.org/10.1021/acs.jpcb.4c00362
J. Phys. Chem. B 2024, 128, 5030−5043

Figure 7. continued

numbers using UV−vis spectroscopy comparisons of two different neutral dye molecules in $[C_4C_1Im][A]$ neat ionic liquids;[74] (f) Kamlet−Taft hydrogen-bond acceptor numbers using UV−vis spectroscopy comparisons of two different neutral dye molecules in $[C_4C_1Im][A]$ neat ionic liquids;[75] (g) hydrogen-bond acceptor numbers measured from the chemical shift δ(F) by ^{19}F NMR spectroscopy of a neutral fluorinated dye molecule dissolved in $[C_4C_1Im][A]$ neat ionic liquids;[76] and (h) hydrogen-bond acceptor values for anions measured by titration using UV−vis spectroscopy of three different neutral dye molecules in two different organic solvents (MeCN and $CHCl_3$).[78] Red = cation probes. Green = neutral probes. Circles = measured in neat ILs, the same as $E_B(N_{cation}$ 1s,exp.). Squares = measured diluted in a molecular solvent. Diamonds = calculations.

support the finding that electrostatic interactions explain the anion-dependent interactions (note that a fourth piece of evidence is given in Section 3.4). First, calculations show that the average E_B(C 1s,calc.) values for all four individual carbon atoms that contribute to $E_B(C_{hetero}$ 1s,calc.), i.e., $E_B(C^4$ 1s,calc.), $E_B(C^5$ 1s,calc.), $E_B(C^6$ 1s,calc.), and $E_B(C^7$ 1s,calc.), match the $E_B(C_{hetero}$ 1s,exp.) trend, i.e., $[NTf_2]^-$ > $[SCN]^-$ > Cl^- (Figure 4d−4g). The lowest unoccupied molecular orbital (LUMO) for $[C_4C_1Im]^+$ was found by calculations to be antibonding π-type located on the imidazolium ring,[92] i.e., on the imidazolium ring carbon (C^2, C^4, C^5) and nitrogen atoms. Therefore, if electron donation occurred from a specific anion occupied valence state to a specific cation unoccupied valence state, one would expect the imidazolium ring carbon (C^2, C^4, C^5) and nitrogen (N^1, N^3) atoms to be more affected than the $N-CH_3$ (C^6) and $N-CH_2-CH_2-$ (C^7) carbon atoms, which is not the case. This finding suggests that the XPS-derived anion-dependent interactions for ILs are best explained by electrostatic interactions rather than an anion occupied valence state to a cation unoccupied valence state interaction. Second, cationic E_B all have the same order for these different $[A]^-$, irrespective of the cation identity.[15,16,19−22] These organic cations have both aromatic ($[C_8C_1Im]^+$, $[C_nC_1C_1Im]^+$, $[C_8Py]^+$) and alkyl ($[P_{6,6,6,14}]^+$, $[C_8C_1Pyrr]^+$, tetraalkylammonium) headgroups; if electron donation occurred from a specific anion-occupied valence state to a specific cation-unoccupied valence state, one would expect the identity of the cation and therefore the identity of the cation-unoccupied valence state to be a strong factor. Third, as reported in ref 15, the results for the nonmethylated ($[C_8C_1Im]^+$) versus methylated ($[C_8C_1C_1Im]^+$) imidazolium cations with $[NTf_2]^-$ and Br^- anions rule out (atom-specific electrostatic) hydrogen bonding interactions to explain any trends. Note that these electrostatic interactions are not constrained to any pair of atoms, unlike bonding or hydrogen bonding interactions - which are for specific atom pairs - but result from contributions from all of the atoms in the vicinity of a given site.

The calculated anion size, which is captured by the calculated anion molecular volume (V_{mol}) taken from ref 93, did not linearly correlate with experimental $E_B(N_{cation}$ 1s,exp.) for 17 ILs (Figure 6c). Data for the experimental size of the IL, the molecular volume of one IL ion pair, also did not linearly correlate with experimental $E_B(N_{cation}$ 1s,exp.) for 10 ILs.[15] In ref 15, a linear correlation was noted for six of the smaller, more strongly interacting ILs. However, such a linear correlation is very much not seen in our data, given the inclusion of $[OcSO_4]^-$, which is one of the largest anions (Figure 6c) but one of the strongest interacting anions on our XPS-derived scale (Figure 1c). $[OcSO_4]^-$ is found to be a midrange to strongly interacting anion on other anion interaction strength scales.[68−71,74] A linear correlation was found for eight ILs between anion interaction strength (i.e., donor number) and molar concentration (proportional to the inverse of the IL size).[94] Again, the inclusion of $[OcSO_4]^-$ in the data set in ref 94 would lead to no linear correlation. Therefore, it can be concluded that anion size is a weak factor in determining anion−cation interaction strengths, and factors such as the identity and number of coordinating atoms will be more important.

There is not a linear correlation between the XPS-derived anion-dependent interaction strength scale and anion polarizability, which further supports our finding that the anion-dependent interaction scale has an electrostatic explanation. Most importantly, $E_B(N_{cation}$ 1s,exp.) for $[C_8C_1Im]Cl$ is smaller than that for $[C_8C_1Im]I$,[15] showing that Cl^- interacts more strongly with $[C_8C_1Im]^+$ than I^-, matching to multiple other interaction strength scales;[68,69,74,76−78] however, the polarizability of I^- is far larger than that of Cl^-.[95] As well as anion polarizability, other data are available on polarizability for IL anions, e.g., individual atom polarizabilities[96] and polarizability scaled to the size of the anion.[97] $[B(CN)_4]^-$ is far more polarizable than Cl^- when anion size is taken into account,[97] but $E_B(N_{cation}$ 1s,exp.) for $[C_8C_1Im]Cl$ is smaller than that for $[C_6C_1Im][B(CN)_4]$, showing that $[B(CN)_4]^-$ interacts far more weakly with cations than Cl^- (Figure 2c). For $[PF_6]^-$ versus $[NTf_2]^-$, $E_B(N_{cation}$ 1s,exp.) values are the same,[15,30] but the atomic polarizability for F in $[PF_6]^-$ is much smaller than the atomic polarizability for O in $[NTf_2]^-$.[96] There is currently insufficient data in the literature on Cl- and Br-containing anions to judge whether atom polarizability for this subset of anions correlates with our anion-dependent interaction strength scale.

The data on E_B and electrostatic site potentials highlights an important point that is almost always overlooked when considering experimental XPS data for ILs. A specific atom type for a specific IL gives a relatively large range of calculated E_B and electrostatic site potential values, e.g., for $[C_8C_1Im]$-$[SCN]$, $E_B(C^2$ 1s,calc.) ranges from 287.17 to 288.41 eV (32 C^2 atoms in each simulation box, three configurations equals 96 C^2 atoms), a difference of 1.24 eV (Figure 5h). While experimental XPS can capture average E_B(core,exp.) from fitting and give an insight into the range of E_B(core,exp.) from the peak width in the fitting, this insight from AIMD plus DFT highlights how in liquids, the localized electronic structure varies greatly across the liquid phase and is strongly dependent on the local environment/structure. Furthermore, the variation of 1.24 eV is far greater than the average E_B difference for $E_B(C^2$ 1s,calc.) of 0.51 eV caused by changing from $[C_8C_1Im]Cl$ to $[C_8C_1Im][NTf_2]$. These observations highlight that within even a relatively small number of ions in a simulation box, there is a great deal of range in the localized electronic structure. This variation is important to keep in mind when considering reactivity, which is likely to occur for unusual structures.

Overall, the anion-dependent interaction strength scale can be explained using a simple electrostatic model. Thus, the anion-dependent electrostatic interaction strength scale is a more appropriate name.

https://doi.org/10.1021/acs.jpcb.4c00362
J. Phys. Chem. B 2024, 128, 5030−5043

3.4. Electrostatic Interactions Explain Anion−Cation and Anion−Neutral Molecule Interactions. Our newly established anion-dependent electrostatic interaction strength scale correlates linearly to four different anion−cation interaction strength scales (Figure 7a−d): ^{23}Na NMR spectroscopy of a Na^+ cation,[68] UV−vis spectroscopy of a Cu^{II}-based cation,[70] chemical shifts δ(H) of the C^2−H proton for $[C_4C_1Im]^+$ using ^{1}H NMR spectroscopy,[69,70] and hydrogen-bond basicity calculated using $[C_4C_1Im][A]$ ion pairs in COSMO-RS (COnductor-like Screening MOdel for Real Solvents).[71] Our anion−cation interaction strength scale also correlates linearly with four different anion−neutral molecule interaction strength scales, which are all measures of anion basicity or hydrogen-bond acceptor ability (Figure 7e−7h).

Two anions that are worth noting are Cl^- and $[CH_3CO_2]^-$, which are generally the two strongest interacting anions. These two anions give the same interaction strength on our XPS scale (Figure 2c) but different values on other interaction strength scales (hydrogen-bond basicity (Figure 7b),[17] donor number (Figure 7c),[18] hydrogen-bond acceptor number (Figure 7g),[21] hydrogen-bond acceptor value (Figure 7h).[22]) $[CH_3CO_2]^-$ is the stronger interacting anion on three scales,[18,21,22] and Cl^- is the stronger interacting anion on one scale.[18] These differences are worthy of further investigation.

The linear correlations (Figure 7) strongly indicate that all eight of the anion−probe interaction strength scales are dominated by electrostatic interactions, as our XPS-derived scale is controlled by electrostatic interactions. The anion-dependent interaction strength scale is very likely independent of the probe identity, including both cations and neutral molecules as the probe. This observation provides a fourth piece of evidence to support the finding that electrostatic interactions explain the anion-dependent interactions (pieces of evidence one to three are given in Section 3.3). Furthermore, these linear correlations indicate that all nine of the anion-dependent interaction strength scales considered here are determined by properties of the anion only, i.e., intrinsic properties of the anion. At this stage, we do not have a single anion property, whether experimental or calculated, that captures the strength of the anion-dependent interaction scales, e.g., anion size does not work (Figure 6c). We expect the best chance of finding such an anion property will be through calculations.

4. CONCLUSIONS

Using XPS and AIMD plus DFT, we have gained significant new insights into anion−cation interactions. We have found evidence that the XPS-derived anion-dependent interaction scale is best rationalized by electrostatic interactions and not occupied valence state/unoccupied valence state interactions or polarizability-driven interactions. Hence, we now call this XPS-derived scale an anion-dependent electrostatic interaction strength scale.

The XPS-derived anion-dependent electrostatic interaction strength scale was due to initial-state (i.e., ground-state) effects and not final-state effects. Therefore, the conclusions drawn in the IL XPS literature, based on the assumption that initial-state effects dominate, are likely to be reliable.

Linear correlations were found between the anion-dependent electrostatic interaction strength scale and many other anion-dependent interaction strength scales, including scales measured using IL cations other than imidazolium, inorganic cations, and neutral molecules. These linear correlations strongly suggest that first, the anion−probe interactions are all primarily electrostatic; second, our electrostatic interaction strength scale captures some inherent, intrinsic property of anions, independent of the probe used to measure the interaction strength scale. These cationic and neutral probes are expected to have very different unoccupied valence states; therefore, the similarity of the trends observed for different anions adds further strength to our finding that electrostatic interactions are the key.

We have placed at least 18 anions on the experimental anion-dependent electrostatic interaction scale for the first time, giving an experimental scale made up of 39 anions, including $[SCN]^-$, $[C(CN)_3]^-$, $[B(CN)_4]^-$, and $[HSO_4]^-$. $[InBr_4]^-$ is, along with $[FAP]^-$ and $[InCl_4]^-$, the most weakly interacting anion on our scale, while Cl^-, Br^-, and $[CH_3CO_2]^-$ are the most strongly interacting anions. We judge the effect of the different anions on the cation potential as not huge, smaller than most differences caused by varying covalent bonding in ions.

One recommendation from our results is that if one is using charge scaling to obtain atomic charges for use in MD simulations,[67,98,99] one must consider anion-dependent charge scaling instead of a fixed value of charge scaling that is usually used. Furthermore, our experimental data set should prove excellent for validating calculations, whether that is for DFT of ion pairs/similar scale calculations, MD-DFT, or AIMD plus DFT. Our data set can greatly help answer a key question for such calculations, i.e., "do these calculations capture the anion-dependent interactions correctly?"

■ ASSOCIATED CONTENT

Data Availability Statement

The data underlying this study are openly available in the University of Reading Research Data Archive at https://doi.org/10.17864/1947.001317.

Supporting Information

The Supporting Information is available free of charge at https://pubs.acs.org/doi/10.1021/acs.jpcb.4c00362.

> Ionic liquids studied and synthesis; peak fitting core level XP spectra and charge referencing; demonstrating purity; anion-cation interaction strength scale for 39 different anions; experimental versus calculated core XPS; linear correlations of E_B and ESP; proving that size does not matter strongly to anion interaction strength; $E_B(O_{anion}\ 1s)$ versus $E_B(N_{cation}\ 1s)$; $[A]^-$-dependent $[A]^-$-$[C]^+$ interactions' anion-cation and anion-neutral molecule interactions (PDF)

■ AUTHOR INFORMATION

Corresponding Author

Kevin R. J. Lovelock − *Department of Chemistry, University of Reading, Reading RG6 6DX, U.K.*; orcid.org/0000-0003-1431-269X; Email: k.r.j.lovelock@reading.ac.uk

Authors

Ekaterina Gousseva − *Department of Chemistry, University of Reading, Reading RG6 6DX, U.K.*

Frances K. Towers Tompkins − *Department of Chemistry, University of Reading, Reading RG6 6DX, U.K.*

Jake M. Seymour − *Department of Chemistry, University of Reading, Reading RG6 6DX, U.K.*

Lewis G. Parker − *Department of Chemistry, University of Reading, Reading RG6 6DX, U.K.;* orcid.org/0000-0001-8727-4116

Coby J. Clarke − *School of Chemistry, University of Nottingham, Nottingham NG7 2RD, U.K.;* orcid.org/0000-0003-2698-3490

Robert G. Palgrave − *Department of Chemistry, University College London, London WC1H 0AJ, U.K.;* orcid.org/0000-0003-4522-2486

Roger A. Bennett − *Department of Chemistry, University of Reading, Reading RG6 6DX, U.K.;* orcid.org/0000-0001-6266-3510

Ricardo Grau-Crespo − *Department of Chemistry, University of Reading, Reading RG6 6DX, U.K.;* orcid.org/0000-0001-8845-1719

Complete contact information is available at: https://pubs.acs.org/10.1021/acs.jpcb.4c00362

Notes

The authors declare no competing financial interest.

■ ACKNOWLEDGMENTS

The authors are grateful to the U.K. Materials and Molecular Modelling Hub for access to the Young supercomputer facility, which is partially funded by the EPSRC (EP/T022213/1). This work also used the ARCHER2 U.K. National Supercomputing Service via the Materials Chemistry Consortium, which is also funded by EPRSC (EP/R029431/1). K.R.J.L. acknowledges support from a Royal Society University Research Fellowship (URF\R\150353 and URF\R\211005). J.M.S. acknowledges support from a Royal Society University Research Fellowship Enhancement Award (RGF\EA\180089). E.G. acknowledges support from a Royal Society Research Grant for Research Fellows (RGF\R1\180053). L.G.P. and F.K.T.T. acknowledge support from a Royal Society Research Fellows Enhanced Research Expenses (RF\ERE\210061). K.R.J.L. acknowledges support from an EPSRC Capital Award for Early Career Researchers. Dr. Richard Matthews is thanked for helpful discussions.

■ REFERENCES

(1) Ueno, K.; Tokuda, H.; Watanabe, M. Ionicity in ionic liquids: correlation with ionic structure and physicochemical properties. *Phys. Chem. Chem. Phys.* **2010**, *12* (8), 1649−1658.

(2) Lovelock, K. R. J. Quantifying intermolecular interactions of ionic liquids using cohesive energy densities. *R. Soc. Open Sci.* **2017**, *4* (12), No. 171223.

(3) Armand, M.; Endres, F.; MacFarlane, D. R.; Ohno, H.; Scrosati, B. Ionic-liquid materials for the electrochemical challenges of the future. *Nat. Mater.* **2009**, *8* (8), 621−629.

(4) MacFarlane, D. R.; Tachikawa, N.; Forsyth, M.; Pringle, J. M.; Howlett, P. C.; Elliott, G. D.; Davis, J. H.; Watanabe, M.; Simon, P.; Angell, C. A. Energy applications of ionic liquids. *Energy Environ. Sci.* **2014**, *7* (1), 232−250.

(5) MacFarlane, D. R.; Forsyth, M.; Howlett, P. C.; Kar, M.; Passerini, S.; Pringle, J. M.; Ohno, H.; Watanabe, M.; Yan, F.; Zheng, W. J.; et al. Ionic liquids and their solid-state analogues as materials for energy generation and storage. *Nat. Rev. Mater.* **2016**, *1* (2), No. 15005.

(6) Abbott, A. P.; McKenzie, K. J. Application of ionic liquids to the electrodeposition of metals. *Phys. Chem. Chem. Phys.* **2006**, *8* (37), 4265−4279.

(7) Shiddiky, M. J. A.; Torriero, A. A. J. Application of ionic liquids in electrochemical sensing systems. *Biosens. Bioelectron.* **2011**, *26* (5), 1775−1787.

(8) Brennecke, J. F.; Gurkan, B. E. Ionic Liquids for CO2 Capture and Emission Reduction. *J. Phys. Chem. Lett.* **2010**, *1* (24), 3459−3464.

(9) Hallett, J. P.; Welton, T. Room-Temperature Ionic Liquids: Solvents for Synthesis and Catalysis. 2. *Chem. Rev.* **2011**, *111* (5), 3508−3576.

(10) Li, Z.; Dewulf, B.; Binnemans, K. Nonaqueous Solvent Extraction for Enhanced Metal Separations: Concept, Systems, and Mechanisms. *Ind. Eng. Chem. Res.* **2021**, *60* (48), 17285−17302.

(11) Binnemans, K.; Jones, P. T. Ionic Liquids and Deep-Eutectic Solvents in Extractive Metallurgy: Mismatch Between Academic Research and Industrial Applicability. *J. Sustainable Metall.* **2023**, *9* (2), 423−438.

(12) Lovelock, K. R. J.; Villar-Garcia, I. J.; Maier, F.; Steinrück, H. P.; Licence, P. Photoelectron Spectroscopy of Ionic Liquid-Based Interfaces. *Chem. Rev.* **2010**, *110* (9), 5158−5190.

(13) Lovelock, K. R. J.; Licence, P. Ionic Liquids Studied at Ultra-High Vacuum. In *Ionic Liquids UnCoiled: Critical Expert Overviews*; Seddon, K. R.; Plechkova, N. V., Eds.; Wiley, 2012; pp 251−282.

(14) Steinrück, H.-P. Recent developments in the study of ionic liquid interfaces using X-ray photoelectron spectroscopy and potential future directions. *Phys. Chem. Chem. Phys.* **2012**, *14* (15), 5010−5029.

(15) Cremer, T.; Kolbeck, C.; Lovelock, K. R. J.; Paape, N.; Wölfel, R.; Schulz, P. S.; Wasserscheid, P.; Weber, H.; Thar, J.; Kirchner, B.; et al. Towards a Molecular Understanding of Cation-Anion Interactions-Probing the Electronic Structure of Imidazolium Ionic Liquids by NMR Spectroscopy, X-ray Photoelectron Spectroscopy and Theoretical Calculations. *Chem. - Eur. J.* **2010**, *16* (30), 9018−9033.

(16) Hurisso, B. B.; Lovelock, K. R. J.; Licence, P. Amino acid-based ionic liquids: using XPS to probe the electronic environment via binding energies. *Phys. Chem. Chem. Phys.* **2011**, *13* (39), 17737−17748.

(17) Taylor, A. W.; Men, S.; Clarke, C. J.; Licence, P. Acidity and basicity of halometallate-based ionic liquids from X-ray photoelectron spectroscopy. *RSC Adv.* **2013**, *3* (24), 9436−9445.

(18) Men, S. A.; Lovelock, K. R. J.; Licence, P. X-ray photoelectron spectroscopy of trihalide ionic liquids: Comparison to halide-based analogues, anion basicity and beam damage. *Chem. Phys. Lett.* **2017**, *679*, 207−211.

(19) Men, S.; Mitchell, D. S.; Lovelock, K. R. J.; Licence, P. X-ray Photoelectron Spectroscopy of Pyridinium-Based Ionic Liquids: Comparison to Imidazolium- and Pyrrolidinium-Based Analogues. *ChemPhysChem* **2015**, *16* (10), 2211−2218.

(20) Men, S.; Jin, Y. J.; Licence, P. Probing the impact of the N3-substituted alkyl chain on the electronic environment of the cation and the anion for 1,3-dialkylimidazolium ionic liquids. *Phys. Chem. Chem. Phys.* **2020**, *22* (30), 17394−17400.

(21) Blundell, R. K.; Licence, P. Quaternary ammonium and phosphonium based ionic liquids: a comparison of common anions. *Phys. Chem. Chem. Phys.* **2014**, *16* (29), 15278−15288.

(22) Men, S.; Lovelock, K. R. J.; Licence, P. X-ray photoelectron spectroscopy of pyrrolidinium-based ionic liquids: cation-anion interactions and a comparison to imidazolium-based analogues. *Phys. Chem. Chem. Phys.* **2011**, *13* (33), 15244−15255.

(23) Hohlneicher, G.; Pulm, H.; Freund, H. J. On the separation of initial and final state effects in photoelectron spectroscopy using an extension of the auger-parameter concept. *J. Electron Spectrosc. Relat. Phenom.* **1985**, *37* (3), 209−224.

(24) Egelhoff, W. F. Core-level binding-energy shifts at surfaces and in solids. *Surf. Sci. Rep.* **1987**, *6* (6−8), 253−415.

(25) Kolasinski, K. W. *Surface Science: Foundations of Catalysis and Nanoscience*; Wiley, 2020.

(26) Briggs, D.; Grant, J. T. *Surface Analysis by Auger and X-ray Photoelectron Spectroscopy*; IM Publications: Manchester, 2003.

(27) Lovelock, K. R. J.; Kolbeck, C.; Cremer, T.; Paape, N.; Schulz, P. S.; Wasserscheid, P.; Maier, F.; Steinrück, H. P. Influence of Different Substituents on the Surface Composition of Ionic Liquids Studied Using ARXPS. *J. Phys. Chem. B* **2009**, *113* (9), 2854−2864.
(28) Taylor, A. W.; Qiu, F. L.; Villar-Garcia, I. J.; Licence, P. Spectroelectrochemistry at ultrahigh vacuum: in situ monitoring of electrochemically generated species by X-ray photoelectron spectroscopy. *Chem. Commun.* **2009**, No. 39, 5817−5819.
(29) Apperley, D. C.; Hardacre, C.; Licence, P.; Murphy, R. W.; Plechkova, N. V.; Seddon, K. R.; Srinivasan, G.; Swadźba-Kwaśny, M.; Villar-Garcia, I. J. Speciation of chloroindate(III) ionic liquids. *Dalton Trans.* **2010**, *39* (37), 8679−8687.
(30) Villar-Garcia, I. J.; Smith, E. F.; Taylor, A. W.; Qiu, F. L.; Lovelock, K. R. J.; Jones, R. G.; Licence, P. Charging of ionic liquid surfaces under X-ray irradiation: the measurement of absolute binding energies by XPS. *Phys. Chem. Chem. Phys.* **2011**, *13* (7), 2797−2808.
(31) Reinmöller, M.; Ulbrich, A.; Ikari, T.; Preiss, J.; Höfft, O.; Endres, F.; Krischok, S.; Beenken, W. J. D. Theoretical reconstruction and elementwise analysis of photoelectron spectra for imidazolium-based ionic liquids. *Phys. Chem. Chem. Phys.* **2011**, *13* (43), 19526−19533.
(32) Taccardi, N.; Niedermaier, I.; Maier, F.; Steinrück, H. P.; Wasserscheid, P. Cyclic Thiouronium Ionic Liquids: Physicochemical Properties and their Electronic Structure Probed by X-Ray Induced Photoelectron Spectroscopy. *Chem. - Eur. J.* **2012**, *18* (27), 8288−8291.
(33) Villar-Garcia, I. J.; Lovelock, K. R. J.; Men, S.; Licence, P. Tuning the electronic environment of cations and anions using ionic liquid mixtures. *Chem. Sci.* **2014**, *5* (6), 2573−2579.
(34) Blundell, R. K.; Licence, P. Tuning cation-anion interactions in ionic liquids by changing the conformational flexibility of the cation. *Chem. Commun.* **2014**, *50* (81), 12080−12083.
(35) Santos, A. R.; Blundell, R. K.; Licence, P. XPS of guanidinium ionic liquids: a comparison of charge distribution in nitrogenous cations. *Phys. Chem. Chem. Phys.* **2015**, *17* (17), 11839−11847.
(36) Longo, L. S.; Smith, E. F.; Licence, P. Study of the Stability of 1-Alkyl-3-methylimidazolium Hexafluoroantimonate(V) Based Ionic Liquids Using X-ray Photoelectron Spectroscopy. *ACS Sustainable Chem. Eng.* **2016**, *4* (11), 5953−5962.
(37) Santos, A. R.; Hanson-Heine, M. W. D.; Besley, N. A.; Licence, P. The impact of sulfur functionalisation on nitrogen-based ionic liquid cations. *Chem. Commun.* **2018**, *54* (81), 11403−11406.
(38) Heller, B. S. J.; Kolbeck, C.; Niedermaier, I.; Dommer, S.; Schatz, J.; Hunt, P.; Maier, F.; Steinrück, H. P. Surface Enrichment in Equimolar Mixtures of Non-Functionalized and Functionalized Imidazolium-Based Ionic Liquids. *ChemPhysChem* **2018**, *19* (14), 1733−1745.
(39) Men, S.; Licence, P.; Do-Thanh, C. L.; Luo, H. M.; Dai, S. X-ray photoelectron spectroscopy of piperidinium ionic liquids: a comparison to the charge delocalised pyridinium analogues. *Phys. Chem. Chem. Phys.* **2020**, *22* (21), 11976−11983.
(40) Men, S.; Licence, P.; Luo, H. M.; Dai, S. Tuning the Cation-Anion Interactions by Methylation of the Pyridinium Cation: An X-ray Photoelectron Spectroscopy Study of Picolinium Ionic Liquids. *J. Phys. Chem. B* **2020**, *124* (30), 6657−6663.
(41) Clarke, C. J.; Maxwell-Hogg, S.; Smith, E. F.; Hawker, R. R.; Harper, J. B.; Licence, P. Resolving X-ray photoelectron spectra of ionic liquids with difference spectroscopy. *Phys. Chem. Chem. Phys.* **2019**, *21* (1), 114−123.
(42) Dick, E. J.; Fouda, A. E. A.; Besley, N. A.; Licence, P. Probing the electronic structure of ether functionalised ionic liquids using X-ray photoelectron spectroscopy. *Phys. Chem. Chem. Phys.* **2020**, *22* (3), 1624−1631.
(43) Fogarty, R. M.; Matthews, R. P.; Ashworth, C. R.; Brandt-Talbot, A.; Palgrave, R. G.; Bourne, R. A.; Hoogerstraete, T. V.; Hunt, P. A.; Lovelock, K. R. J. Experimental validation of calculated atomic charges in ionic liquids. *J. Chem. Phys.* **2018**, *148* (19), No. 193817.
(44) Fogarty, R. M.; Rowe, R.; Matthews, R. P.; Clough, M. T.; Ashworth, C. R.; Brandt, A.; Corbett, P. J.; Palgrave, R. G.; Smith, E. F.; Bourne, R. A.; et al. Atomic charges of sulfur in ionic liquids: experiments and calculations. *Faraday Discuss.* **2018**, *206*, 183−201.
(45) Rangan, S.; Viereck, J.; Bartynski, R. A. Electronic Properties of Cyano Ionic Liquids: a Valence Band Photoemission Study. *J. Phys. Chem. B* **2020**, *124* (36), 7909−7917.
(46) Men, S.; Lovelock, K. R. J.; Licence, P. Directly probing the effect of the solvent on a catalyst electronic environment using X-ray photoelectron spectroscopy. *RSC Adv.* **2015**, *5* (45), 35958−35965.
(47) Men, S.; Jiang, J. X-ray photoelectron spectroscopy as a probe of the interaction between rhodium acetate and ionic liquids. *Chem. Phys. Lett.* **2016**, *646*, 125−129.
(48) Men, S.; Lovelock, K. R. J.; Licence, P. X-ray photoelectron spectroscopy as a probe of rhodium-ligand interaction in ionic liquids. *Chem. Phys. Lett.* **2016**, *645*, 53−58.
(49) Men, S.; Jiang, J. Probing the impact of the cation acidity on the cation-anion interaction in ionic liquids by X-ray photoelectron spectroscopy. *Chem. Phys. Lett.* **2017**, *677*, 60−64.
(50) Men, S.; Jiang, J.; Licence, P. Spectroscopic analysis of 1-butyl-2,3-dimethylimidazolium ionic liquids: Cation-anion interactions. *Chem. Phys. Lett.* **2017**, *674*, 86−89.
(51) Men, S.; Jiang, J.; Liu, Y. X-Ray Photoelectron Spectroscopy of Imidazolium Zwitterionic Salts: Comparison to Acetate Analogs and the Impact of the Alkyl Chain Length on the Charge Distribution. *J. Appl. Spectrosc.* **2017**, *84* (5), 906−910.
(52) Men, S.; Licence, P. Tuning the electronic environment of the anion by using binary ionic liquid mixtures. *Chem. Phys. Lett.* **2017**, *681*, 40−43.
(53) Men, S.; Licence, P. Probing the electronic environment of binary and ternary ionic liquid mixtures by X-ray photoelectron spectroscopy. *Chem. Phys. Lett.* **2017**, *686*, 74−77.
(54) Liu, Y. H.; Ma, C.; Men, S.; Jin, Y. J. An investigation of trioctylmethylammonium ionic liquids by X-ray photoelectron spectroscopy: The cation-anion interaction. *J. Electron Spectrosc. Relat. Phenom.* **2018**, *223*, 79−83.
(55) Men, S.; Jiang, J. Probing the Formation of the NHC-Palladium Species in Ionic Liquids by X-ray Photoelectron Spectroscopy. *Russ. J. Phys. Chem. A* **2018**, *92* (8), 1627−1630.
(56) Men, S.; Jiang, J. X-Ray Photoelectron Spectroscopy of Chlorometallate Ionic Liquids: Speciation and Anion Basicity. *J. Appl. Spectrosc.* **2018**, *85* (1), 55−60.
(57) Men, S.; Jin, Y. J. X-ray Photoelectron Spectroscopy of Imidazolium-Based Zwitterions: The Intramolecular Charge-Transfer Effect. *Russ. J. Phys. Chem. A* **2018**, *92* (11), 2337−2340.
(58) Men, S.; Rong, J. S.; Zhang, T. T.; Wang, X. T.; Feng, L.; Liu, C.; Jin, Y. J. Spectroscopic Analysis of 1-Butyl-3-methylimidazolium Ionic Liquids: Selection of the Charge Reference and the Electronic Environment. *Russ. J. Phys. Chem. A* **2018**, *92* (10), 1975−1979.
(59) Liu, Y. H.; Chen, X. Z.; Men, S.; Licence, P.; Xi, F.; Ren, Z.; Zhu, W. W. The impact of cation acidity and alkyl substituents on the cation-anion interactions of 1-alkyl-2,3-dimethylimidazolium ionic liquids. *Phys. Chem. Chem. Phys.* **2019**, *21* (21), 11058−11065.
(60) Wei, L.; Men, S. X-ray Photoelectron Spectroscopy of 1-Butyl-2,3-Dimethylimidazolium Ionic Liquids: Charge Correction Methods and Electronic Environment of the Anion. *Russ. J. Phys. Chem. A* **2019**, *93* (13), 2676−2680.
(61) He, Y.; Men, S. Charge Distribution of Phosphonium Ionic Liquids: Phosphonium versus Phosphate. *Russ. J. Phys. Chem. A* **2020**, *94* (10), 2091−2095.
(62) Mu, R.; Deng, A. M.; Men, S. Tribromide Ionic Liquids: Probing the Charge Distribution of the Anion by XPS. *Russ. J. Phys. Chem. A* **2020**, *94* (5), 1053−1056.
(63) Wei, L.; Wang, S. Q.; Men, S. Electronic Effects in the Structure of 1-Ethyl-3-Methylimidazolium Ionic Liquids. *Russ. J. Phys. Chem. A* **2021**, *95* (4), 736−740.
(64) Men, S.; Sun, Y. S.; Licence, P.; Qu, J. X-ray photoelectron spectroscopy of morpholinium ionic liquids: impact of a long alkyl side substituent on the cation-anion interactions. *Phys. Chem. Chem. Phys.* **2022**, *24* (40), 24845−24851.

https://doi.org/10.1021/acs.jpcb.4c00362
J. Phys. Chem. B 2024, 128, 5030−5043

(65) Lembinen, M.; Nommiste, E.; Ers, H.; Docampo-Alvarez, B.; Kruusma, J.; Lust, E.; Ivanistsev, V. B. Calculation of core-level electron spectra of ionic liquids. *Int. J. Quantum Chem.* **2020**, *120* (14), No. e26247.
(66) Gousseva, E.; Midgley, S. D.; Seymour, J. M.; Seidel, R.; Grau-Crespo, R.; Lovelock, K. R. J. Understanding X-ray Photoelectron Spectra of Ionic Liquids: Experiments and Simulations of 1-Butyl-3-methylimidazolium Thiocyanate. *J. Phys. Chem. B* **2022**, *126* (49), 10500−10509.
(67) Philippi, F.; Goloviznina, K.; Gong, Z.; Gehrke, S.; Kirchner, B.; Padua, A. A. H.; Hunt, P. A. Charge transfer and polarisability in ionic liquids: a case study. *Phys. Chem. Chem. Phys.* **2022**, *24* (5), 3144−3162.
(68) Schmeisser, M.; Illner, P.; Puchta, R.; Zahl, A.; van Eldik, R. Gutmann Donor and Acceptor Numbers for Ionic Liquids. *Chem. - Eur. J.* **2012**, *18* (35), 10969−10982.
(69) Lungwitz, R.; Spange, S. A hydrogen bond accepting (HBA) scale for anions, including room temperature ionic liquids. *New J. Chem.* **2008**, *32* (3), 392−394.
(70) Holzweber, M.; Lungwitz, R.; Doerfler, D.; Spange, S.; Koel, M.; Hutter, H.; Linert, W. Mutual Lewis Acid-Base Interactions of Cations and Anions in Ionic Liquids. *Chem. - Eur. J.* **2013**, *19* (1), 288−293. Article
(71) Cláudio, A. F. M.; Swift, L.; Hallett, J. P.; Welton, T.; Coutinho, J. A. P.; Freire, M. G. Extended scale for the hydrogen-bond basicity of ionic liquids. *Phys. Chem. Chem. Phys.* **2014**, *16* (14), 6593−6601.
(72) Lungwitz, R.; Strehmel, V.; Spange, S. The dipolarity/polarisability of 1-alkyl-3-methylimidazolium ionic liquids as function of anion structure and the alkyl chain length. *New J. Chem.* **2010**, *34* (6), 1135−1140.
(73) Lungwitz, R.; Spange, S. Determination of Hydrogen-Bond-Accepting and -Donating Abilities of Ionic Liquids with Halogeno Complex Anions by Means of 1H NMR Spectroscopy. *ChemPhysChem* **2012**, *13* (7), 1910−1916.
(74) Spange, S.; Lungwitz, R.; Schade, A. Correlation of molecular structure and polarity of ionic liquids. *J. Mol. Liq.* **2014**, *192*, 137−143.
(75) Rani, M. A. A.; Brandt, A.; Crowhurst, L.; Dolan, A.; Hassan, N. H.; Hallett, J. P.; Hunt, P. A.; Lui, M.; Niedermeyer, H.; Perez-Arlandis, J. M.; et al. Understanding the polarity of ionic liquids. *Phys. Chem. Chem. Phys.* **2011**, *13* (37), 16831−16840.
(76) Laurence, C.; Mansour, S.; Vuluga, D.; Legros, J. Measurement of the hydrogen bond acceptance of ionic liquids and green solvents by the F-19 solvatomagnetic comparison method. *Green Chem.* **2021**, *23* (4), 1816−1822.
(77) Galland, N.; Laurence, C.; Le Questel, J. Y. The pK(BHX)-Hydrogen-Bond Basicity Scale: From Molecules to Anions. *J. Org. Chem.* **2022**, *87* (11), 7264−7273.
(78) Pike, S. J.; Hutchinson, J. J.; Hunter, C. A. H-Bond Acceptor Parameters for Anions. *J. Am. Chem. Soc.* **2017**, *139* (19), 6700−6706.
(79) Clarke, C. J.; Hayama, S.; Hawes, A.; Hallett, J. P.; Chamberlain, T. W.; Lovelock, K. R. J.; Besley, N. A. Zinc 1s Valence-to-Core X-ray Emission Spectroscopy of Halozincate Complexes. *J. Phys. Chem. A* **2019**, *123* (44), 9552−9559.
(80) Kolbeck, C.; Killian, M.; Maier, F.; Paape, N.; Wasserscheid, P.; Steinrück, H. P. Surface characterization of functionalized imidazolium-based ionic liquids. *Langmuir* **2008**, *24* (17), 9500−9507.
(81) Seymour, J. M.; Gousseva, E.; Large, A. I.; Clarke, C. J.; Licence, P.; Fogarty, R. M.; Duncan, D. A.; Ferrer, P.; Venturini, F.; Bennett, R. A.; et al. Experimental measurement and prediction of ionic liquid ionisation energies. *Phys. Chem. Chem. Phys.* **2021**, *23* (37), 20957−20973.
(82) Perdew, J. P.; Burke, K.; Ernzerhof, M. Generalized gradient approximation made simple. *Phys. Rev. Lett.* **1996**, *77* (18), 3865−3868.
(83) Grimme, S. Accurate description of van der Waals complexes by density functional theory including empirical corrections. *J. Comput. Chem.* **2004**, *25* (12), 1463−1473.
(84) Grimme, S. Semiempirical GGA-type density functional constructed with a long-range dispersion correction. *J. Comput. Chem.* **2006**, *27* (15), 1787−1799.
(85) Blöchl, P. E. Projector Augmented-Wave Method. *Phys. Rev. B* **1994**, *50* (24), 17953−17979.
(86) Kresse, G.; Furthmüller, J. Efficient iterative schemes for ab initio total-energy calculations using a plane-wave basis set. *Phys. Rev. B* **1996**, *54* (16), 11169−11186.
(87) Kresse, G.; Joubert, D. From ultrasoft pseudopotentials to the projector augmented-wave method. *Phys. Rev. B* **1999**, *59* (3), 1758−1775.
(88) Shkrob, I. A.; Marin, T. W.; Zhu, Y.; Abraham, D. P. Why Bis(fluorosulfonyl)imide Is a "Magic Anion" for Electrochemistry. *J. Phys. Chem. C* **2014**, *118* (34), 19661−19671.
(89) Seymour, J. M.; Gousseva, E.; Tompkins, F. T.; Parker, L.; Alblewi, N.; Clarke, C. J.; Hayama, S.; Palgrave, R.; Bennett, R.; Matthews, R. P.; Lovelock, K. R. J. Unravelling the complex speciation of halozincate ionic liquids using X-ray spectroscopies and calculations *Faraday Discuss.* 2024, Accepted Manuscript, DOI: 10.1039/D4FD00029C.
(90) Vickerman, J. C.; Gilmore, I. S. *Surface Analysis: The Principal Techniques*, 2nd ed.; John Wiley & Sons: Chichester, 2009.
(91) Gupta, V.; Ganegoda, H.; Engelhard, M. H.; Terry, J.; Linford, M. R. Assigning Oxidation States to Organic Compounds via Predictions from X-ray Photoelectron Spectroscopy: A Discussion of Approaches and Recommended Improvements. *J. Chem. Educ.* **2014**, *91* (2), 232−238.
(92) Hunt, P. A.; Kirchner, B.; Welton, T. Characterising the electronic structure of ionic liquids: An examination of the 1-butyl-3-methylimidazolium chloride ion pair. *Chem. - Eur. J.* **2006**, *12* (26), 6762−6775.
(93) Jacquemin, J.; Ge, R.; Nancarrow, P.; Rooney, D. W.; Gomes, M. F. C.; Pádua, A. A. H.; Hardacre, C. Prediction of ionic liquid properties. I. Volumetric properties as a function of temperature at 0.1 MPa. *J. Chem. Eng. Data* **2008**, *53* (3), 716−726.
(94) Weiß, N.; Thielemann, G.; Nagel, K.; Schmidt, C. H.; Seifert, A.; Kassner, L.; Strehmel, V.; Corzilius, B.; Schröder, C.; Spange, S. The influence of the cation structure on the basicity-related polarity of ionic liquids. *Phys. Chem. Chem. Phys.* **2021**, *23* (47), 26750−26760.
(95) Heid, E.; Heindl, M.; Dienstl, P.; Schröder, C. Additive polarizabilities of halides in ionic liquids and organic solvents. *J. Chem. Phys.* **2018**, *149* (4), No. 044302.
(96) Heid, E.; Szabadi, A.; Schröder, C. Quantum mechanical determination of atomic polarizabilities of ionic liquids. *Phys. Chem. Chem. Phys.* **2018**, *20* (16), 10992−10996.
(97) Rodríguez-Fernández, C. D.; Lago, E. L.; Schröder, C.; Varela, L. M. Non-additive electronic polarizabilities of ionic liquids: Charge delocalization effects. *J. Mol. Liq.* **2022**, *346*, No. 117099.
(98) Hollóczki, O.; Malberg, F.; Welton, T.; Kirchner, B. On the origin of ionicity in ionic liquids. Ion pairing versus charge transfer. *Phys. Chem. Chem. Phys.* **2014**, *16* (32), 16880−16890.
(99) Cui, K.; Yethiraj, A.; Schmidt, J. R. Influence of Charge Scaling on the Solvation Properties of Ionic Liquid Solutions. *J. Phys. Chem. B* **2019**, *123* (43), 9222−9229.

https://doi.org/10.1021/acs.jpcb.4c00362
J. Phys. Chem. B 2024, 128, 5030−5043